

Implementation of Enhanced Shape Functions for Non-Affine Elements

Gaëlle Andriamaro¹, Oleg Davydov², and John Simkin³

¹University of Strathclyde, gaelle.andriamaro@strath.ac.uk

²University of Giessen, Oleg.Davydov@math.uni-giessen.de

³Cobham CTS, John.Simkin@cobham.com

Abstract

The performance of different edge vector basis functions is compared for non-affine elements. Improved accuracy is measured by comparing the calculated eigenvalues of the electromagnetic field distribution in a cavity with analytical results. Enhanced $H(\text{curl})$ -conforming basis functions are numerically shown to preserve the optimal approximation properties of the finite element on non-affine hexahedra.

1 Introduction

Edge elements are well suited to the analysis of electromagnetic fields for both the quasi static and high frequency limits of Maxwell's equations. Simplicial elements using Nédélec edge basis functions give stable, convergent solutions provided that the element shapes are not too extreme [6]. Other elements types, for example triangular prisms, pyramids and hexahedra, can be constructed using the Nédélec family of edge vector basis functions. However, the shape of these elements has a strong effect on the accuracy [2, 5, 3]. Modified edge basis functions have been developed to resolve the problem [10] but these are costly to calculate.

Enhanced edge vector basis functions have recently been proposed [9, 3]. This paper discusses an implementation of these enhanced hierarchical basis functions for hexahedral elements, and provides numerical comparison to the classical Nédélec basis functions. The enhanced basis functions are easy to calculate and include additional face- and volume-based degrees of freedom. In addition to the Nédélec degrees of freedom, each enhanced hexahedron has two degrees of freedom per face, and three internal degrees of freedom, as displayed on Figure 1. The face-based degrees of freedom are shared on the element interface. The rationale behind the construction of the extended edge elements is based on a local-to-global mapping analysis,

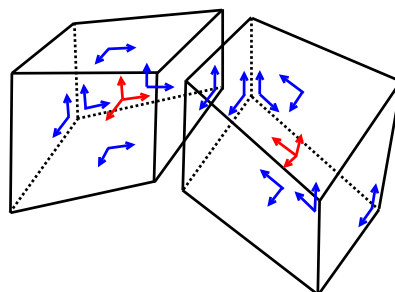


Figure 1: Additional Hexahedral Degrees of Freedom.

and is discussed in Section 2.

In this paper the eigenvalues of the electromagnetic field in a cavity are used to investigate the solution errors that are related to non-affine element shapes. The results are obtained using Opera SOPRANO [1] for the computation of high-frequency electromagnetic fields and ARPACK [11] to calculate eigenvalues. Timings were taken using a 3.6 GHz Intel Xeon E5-1620.

Nédélec elements [13] are needed for electromagnetics problems for which it has been established that nodal (piecewise continuous) elements yield non-physical solutions [14, 7]. In contrast to nodal elements, Nédélec elements, also referred to as tangential

elements, are characterized by tangential continuity across the elements interface and as such, provide the natural framework for solving finite element discretizations of variational problems in electromagnetics (cf. [4, 15, 12] and the references therein).

Finite elements are typically constructed on a so-called *reference element* with ideal symmetry properties, such as a unit cube or a symmetric pyramid. The global finite elements are then generated by applying appropriate differential mappings and enforcing suitable continuity conditions across the elements interface. Affine elements are obtained by affine transformations of reference elements with a constant Jacobian. On fully affine meshes, Nédélec elements of order r are proved to yield an optimal convergence rate in $H(\text{curl})$ -norm [8].

This optimality is lost when the elements do not tend to an affine mesh, as the mesh is refined. In order to retain the optimal approximation properties on non-affine meshes, the Nédélec shape functions need to be augmented [9, 3]. The purpose of this work is to demonstrate the effectiveness of the enhanced edge elements on non-affine meshes.

This paper is organized as follows. The theoretical conditions for optimal accuracy and the motivation behind the extension of the Nédélec are discussed in Section 2. In order to enforce $H(\text{curl})$ -conformity, the extended finite element space must be tangentially continuous, which is done by adopting a unique *global* orientation of the shape functions whose tangential components do not vanish on the elements interface. The enhanced edge elements include additional face-based degrees of freedom with non-zero tangential components across the element's faces. An easy and efficient solution for addressing the non-trivial orientation of these additional face-based degrees of freedom is discussed in Section 3. Section 4 contains numerical simulations which compare the performance of the enhanced edge elements with that of the Nédélec elements. The main results are summarized in Section 5.

2 Rationale

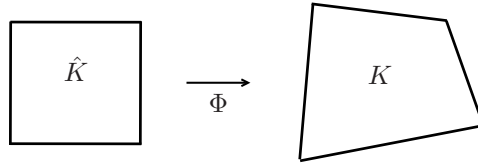


Figure 2: Local-to-Global Mapping.

As mentioned previously, finite elements are typically constructed from a reference element by means of appropriate differential mappings. Assuming that the reference element \hat{K} and the physical element K are related by a diffeomorphism Φ such that $\Phi(\hat{K}) = K$ (as shown on Figure 2 for a non-affine quadrilateral), then the vector fields are related by the $H(\text{curl})$ -conforming transform [2, Equation (1.3)]:

$$\hat{\mathbf{A}}(\hat{\mathbf{x}}) = d\Phi(\hat{\mathbf{x}})^{\text{tr}} \mathbf{A}(\mathbf{x}),$$

or, alternatively,

$$\mathbf{A}(\mathbf{x}) = d\Phi(\hat{\mathbf{x}})^{-\text{tr}} \hat{\mathbf{A}}(\hat{\mathbf{x}}), \quad (1)$$

where $(\cdot)^{\text{tr}}$ denotes the transpose operator, and $d\Phi$ represents the Jacobian matrix of the transformation.

In order to maintain an optimal approximation in $H(\text{curl})$ -norm, the key idea used in [3] consists in determining which functions need to be added on the reference element, for the Nédélec space to be spanned by the shape functions on the physical element. More precisely, for a given polynomial order r , the vector field \mathbf{A} in Equation (1) is successively substituted with Nédélec polynomials of order r , which, combined with the fact that Φ is a generic non-affine map (trilinear diffeomorphism for hexahedra), yields an extended edge element space for non-affine geometries. In the lowest-order case, the enhanced hexahedral element has two additional degrees of freedom per face, plus three volume-based degrees of freedom, as illustrated on Figure 1. Using an alternative approach based on the de Rham diagram and the optimal L^2 -approximation of $\text{curl}(\mathbf{A})$ in $H(\text{div})$, Falk *et al* [9] construct the same hexahedral basis for the lowest-order case.

On the reference hexahedron $\hat{K} := [0, 1]^3$, the additional lowest-order volume-based shape functions have the following form:

$$\begin{aligned} \hat{\mathbf{E}}_{\hat{x}}^{\text{v}} &= \hat{y}(1 - \hat{y})\hat{z}(1 - \hat{z})\hat{\mathbf{e}}_{\hat{x}}, \\ \hat{\mathbf{E}}_{\hat{y}}^{\text{v}} &= \hat{z}(1 - \hat{z})\hat{x}(1 - \hat{x})\hat{\mathbf{e}}_{\hat{y}}, \\ \hat{\mathbf{E}}_{\hat{z}}^{\text{v}} &= \hat{x}(1 - \hat{x})\hat{y}(1 - \hat{y})\hat{\mathbf{e}}_{\hat{z}}, \end{aligned} \quad (2)$$

where $\hat{\mathbf{e}}_{\hat{x}}$ denote the unit vector along the \hat{x} -axis. The symbols in the last two equations are defined in a similar way. In the above equation, note that $\beta_{f_1, \hat{y}} := \hat{y}$ and $\beta_{f_2, \hat{y}} := 1 - \hat{y}$ are parametrizations of the two faces of \hat{K} which are orthogonal to the \hat{y} -axis. By definition, the parameter β_f associated with a face f orthogonal to the \hat{x}_i -axis is either of the form $\beta_f := \hat{x}_i$ or $\beta_f := 1 - \hat{x}_i$,

and defined in such a way that $\beta_f|_f \equiv 0$. It thus follows that the volume-based shape functions defined in Equation (2) have vanishing tangential components on the element's boundary.

Similarly, the additional lowest-order shape functions associated with the face f , parallel to the $\hat{x}\hat{y}$ -plane, have the following form:

$$\begin{aligned}\hat{\mathbf{E}}_{\hat{x}\hat{y}}^{f,1} &= \hat{y}(1 - \hat{y})\beta_{f'}\hat{\mathbf{e}}_{\hat{x}}, \\ \hat{\mathbf{E}}_{\hat{x}\hat{y}}^{f,2} &= \hat{x}(1 - \hat{x})\beta_{f'}\hat{\mathbf{e}}_{\hat{y}},\end{aligned}\quad (3)$$

where $\beta_{f'}$ represents the parametrization of the face opposite to f . For example, if the face f in the above equation lies on the plane $\hat{z} = 0$ (respectively $1 - \hat{z} = 0$), then $\beta_{f'} := 1 - \hat{z}$ (respectively $\beta_{f'} := \hat{z}$). The shape functions associated with faces lying on the $\hat{y}\hat{z}$ - or $\hat{z}\hat{x}$ -plane have an equivalent form as in Equation (3), that is,

$$\begin{aligned}\hat{\mathbf{E}}_{\hat{y}\hat{z}}^{f,1} &= \hat{z}(1 - \hat{z})\beta_{f'}\hat{\mathbf{e}}_{\hat{y}}, \\ \hat{\mathbf{E}}_{\hat{y}\hat{z}}^{f,2} &= \hat{y}(1 - \hat{y})\beta_{f'}\hat{\mathbf{e}}_{\hat{z}},\end{aligned}$$

and

$$\begin{aligned}\hat{\mathbf{E}}_{\hat{z}\hat{x}}^{f,1} &= \hat{x}(1 - \hat{x})\beta_{f'}\hat{\mathbf{e}}_{\hat{z}}, \\ \hat{\mathbf{E}}_{\hat{z}\hat{x}}^{f,2} &= \hat{z}(1 - \hat{z})\beta_{f'}\hat{\mathbf{e}}_{\hat{x}}.\end{aligned}$$

Again using the fact that a parameter associated with a given face by definition vanish on the face, one can see from Equation (3) that a face-based shape function has vanishing tangential components, except on the corresponding face. Hence, in order to ensure that the resulting finite element approximation is conforming, it is crucial to enforce a consistent orientation of the face-based shape functions between two adjacent elements.

3 Orientation Problem

As discussed in the previous section, the enhanced edge elements include additional degrees of freedom which correspond to the element's faces. In order to ensure the conformity of the resulting finite element approximation, the face-based shape functions need to have a unique *global* parametrization, independently from the element local coordinate system, so as to enforce tangential continuity across the element interface.

One can see from Equation (3) that each lowest-order face-based basis function is parallel to a specific unit vector. Taking advantage of this property would consist in associating a face-based shape function with a unique pair of nodes, as done for the Nédélec basis functions. However, this does not seem possible for the shape functions in Equation (3). Indeed, observe from Equation (3) that each face-based shape function is parallel to two edges of the corresponding face, as displayed on Figure 3.

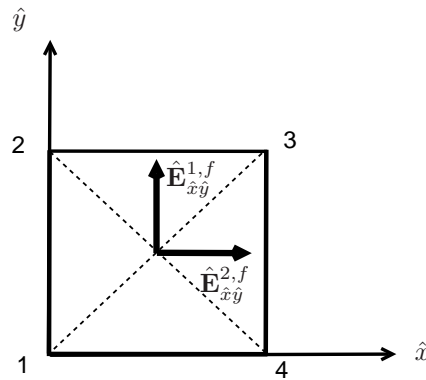


Figure 3: Face-Based Shape Functions.

A simple yet effective way of resolving this consists in replacing the shape functions $\hat{\mathbf{E}}_{\hat{x}\hat{y}}^{f,1}$ and $\hat{\mathbf{E}}_{\hat{x}\hat{y}}^{f,2}$ with $\hat{\Xi}_{\hat{x}\hat{y}}^{f,1}$ and $\hat{\Xi}_{\hat{x}\hat{y}}^{f,2}$ defined by:

$$\begin{aligned}\hat{\Xi}_{\hat{x}\hat{y}}^{f,1} &:= \hat{\mathbf{E}}_{\hat{x}\hat{y}}^{f,1} + \hat{\mathbf{E}}_{\hat{x}\hat{y}}^{f,2}, \\ \hat{\Xi}_{\hat{x}\hat{y}}^{f,2} &:= \hat{\mathbf{E}}_{\hat{x}\hat{y}}^{f,1} - \hat{\mathbf{E}}_{\hat{x}\hat{y}}^{f,2}.\end{aligned}\quad (4)$$

The redefined face-based shape functions $\hat{\Xi}_{\hat{x}\hat{y}}^{f,1}$ and $\hat{\Xi}_{\hat{x}\hat{y}}^{f,2}$ are represented by the dashed arrows on Figure 4.

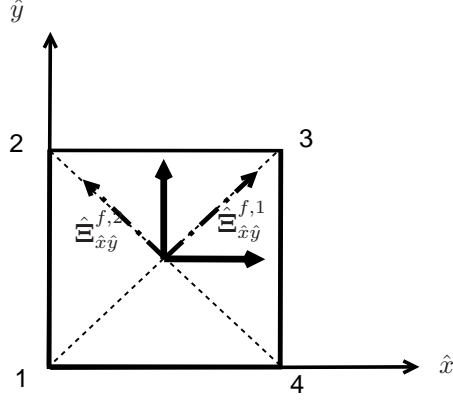


Figure 4: Redefined Face-Based Shape Functions.

As illustrated on Figure 4, making use of the functions defined in Equation (4) yields a very natural one-to-one correspondence between the face-based shape functions and the face diagonals and thus the pairs of their endpoints, thereby facilitating the assembly of the face-based degrees of freedom. This approach also has the advantage of providing a consistency of implementation, which facilitates the integration of the enhanced edge elements with the Nédélec elements in the lowest-order case.

4 Results

The improved effectiveness of the enhanced edge basis over the standard Nédélec basis is demonstrated by computing the eigenvalues of a simple rectangular cavity formulated as follows:

$$\begin{aligned} \nabla \times \nabla \times \mathbf{E} &= \omega^2 \mathbf{E} \quad \text{in } \Omega, \\ \mathbf{E} \times \mathbf{n} &= \mathbf{0} \quad \text{on } \partial\Omega, \end{aligned}$$

where $\Omega := [0, 1/\sqrt[3]{10}]^3$ is the domain, $\partial\Omega$ denotes the boundary of the domain, and \mathbf{E} represents the electric field. It is well-known that the eigenvalues which correspond to the above problem are given by

$$\omega_{k,\ell,m} = \frac{\pi}{\sqrt[3]{10}} \sqrt{k^2 + \ell^2 + m^2}, \quad k, \ell, m \in \mathbb{Z}_0^+. \quad (5)$$

The solution error is measured as the relative error in the frequency of the calculated modes. For the sake of clarity, three non-trivial modes have been selected in the numerical results presented in this section. More precisely, Mode 1, Mode 2 and Mode 3 respectively correspond to $\omega_{1,1,0}$, $\omega_{1,1,1}$ and $\omega_{2,1,1}$.

Using an affine mesh of rectangular shape produces the results displayed in Table 1 and Table 2 below, where h and N respectively denote the element size and the number of elements, and the computational time is measured in seconds:

h	N	dof	time	Error1	Error2	Error3
1	1000	10830	2	6.73e-6	4.07e-3	7.79e-3
0.5	8000	91260	20	4.22e-7	1.03e-3	2.04e-3
0.25	64000	748920	322	2.64e-8	2.57e-4	5.12e-4

Table 1: Relative Frequency Error with Enhanced Elements on the Uniform Mesh.

h	N	dof	time	Error1	Error2	Error3
1	1000	2430	1	4.12e-3	4.12e-3	1.24e-2
0.5	8000	21660	6	1.03e-3	1.03e-3	3.09e-3
0.25	64000	182520	74	2.57e-4	2.57e-4	7.71e-4

Table 2: Relative Frequency Error with Nédélec Elements on the Uniform Mesh.

The convergence order is illustrated in Figure 5, where the thicker lines correspond to the enhanced edge elements.

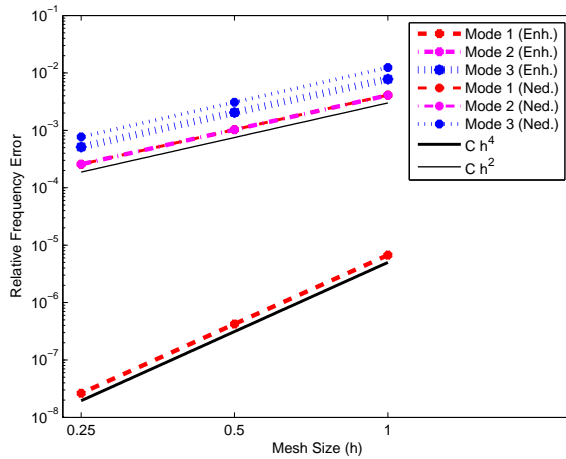


Figure 5: Using a Rectangular Mesh.

Although Mode 1 converges as $\mathcal{O}(h^4)$ with the enhanced elements, the other modes yield the expected convergence rate, when using either the enhanced or the Nédélec elements. In particular, the curves produced by the Nédélec elements for Mode 2 and Mode 3 are hidden behind those obtained using the enhanced edge elements. It is more efficient to use Nédélec elements on affine meshes because they produce fewer degrees of freedom.

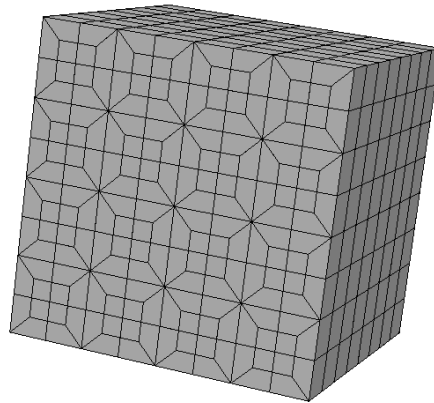


Figure 6: Non-Affine Mesh.

Using the non-affine mesh given in Figure 6 produces the results summarized in Table 3 and Table 4:

h	N	dof	time	Error1	Error2	Error3
2.5	24	272	0.3	1.16e-3	1.12e-2	1.40e-2
1.25	192	2240	0.9	3.21e-4	2.79e-3	4.37e-3
0.625	1536	18176	2.74	8.23e-5	6.98e-4	2.00e-3
0.3125	12288	146432	18	2.07e-5	1.75e-4	2.75e-4
0.15625	98304	1175552	240	5.19e-6	4.37e-5	6.87e-5

Table 3: Relative Frequency Error with Enhanced Elements on the Non-Affine Mesh.

h	N	dof	time	Error1	Error2	Error3
2.5	24	186	0.2	2.41e-2	2.62e-2	6.19e-2
1.25	192	544	0.8	1.14e-2	1.28e-2	1.82e-2
0.625	1536	4480	1.29	8.18e-3	1.03e-2	1.35e-2
0.3125	12288	36352	6.5	7.38e-3	9.69e-3	1.23e-2
0.15625	98304	292864	58.1	7.18e-3	9.53e-3	1.19e-2

Table 4: Relative Frequency Error with Nédélec Elements on the Non-Affine Mesh.

The variation of the error as a function of the mesh size is illustrated on Figure 7:

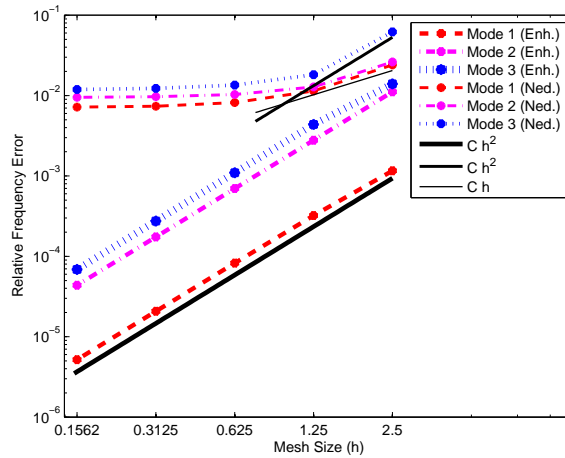


Figure 7: Using a Non-Affine Mesh.

As predicted, Figure 3 shows that the enhanced elements provide a $\mathcal{O}(h^2)$ convergence rate on the non-affine mesh. Figure 7 illustrates the limitations of the Nédélec elements on non-affine meshes. As shown in Table 4, refining the mesh brings no significant improvement on the accuracy produced by the Nédélec elements on the non-affine mesh. Thus, we observe that, on the non-affine mesh, the enhanced edge elements give improved accuracy and faster results, using significantly less degrees of freedom.

5 Conclusion

The enhanced edge elements are specifically designed to optimize the accuracy of the finite element solution on non-affine meshes. This optimization comes with the cost of additional degrees of freedom at the element-level. The bulk of the new degrees of freedom is however shared between adjacent elements. When using affine meshes, it is more efficient to use Nédélec elements, as the inclusion of the additional degrees of freedom has virtually no effect on the produced accuracy. However, on non-affine meshes, the enhanced elements perform significantly better than the Nédélec elements, producing faster and more accurate results for comparable number of degrees of freedom.

Acknowledgements

This work was supported through the short Knowledge Transfer Partnership (sKTP) programme which is led by the Technology Strategy Board (TSB).

References

- [1] "Cobham Technical Services Vector Fields Software".
<http://www.operaFEA.com>.
- [2] D. Arnold, D. Boffi, and R. Falk. Quadrilateral $H(\text{div})$ finite elements. *SIAM J. Numer. Anal.*, 42:2429–2451, 2005.
- [3] M. Bergot and M. Duruflé. High-order optimal edge elements for pyramids, prisms and hexahedra. *J. COMPUT PHYS*, 232:189–213, 2013.
- [4] D. Boffi, P. Fernandes, L. Gastaldi, and I. Perugia. Computational models of electromagnetic resonators: Analysis of edge element approximation. *SIAM J. Numer. Anal.*, 36:1264–1290, 1999.
- [5] D. Boffi, F. Kikushi, and S. Schöberl. Edge element computation of Maxwell's eigenvalues on general quadrilateral meshes. *Math. Mod. Meth. Appl. Sci.*, 16:265–273, 2006.
- [6] F. Brezzi and M. Fortin. Mixed and hybrid finite element methods. *Springer Ser. Comput. Math.*, 15, 1991.

- [7] M. Costabel and M. Dauge. Singularities of electromagnetic fields in polyhedral domains. *Arch. Rational Mech. Anal.*, 151:221–276, 2000.
- [8] L. Demkowicz, J. Kurtz, D. Pardo, M. Paszynski, W. Rachowicz, and W. Zdunek. *Computing with hp-adaptive finite elements: Volume II*. 2007.
- [9] R. Falk, P. Gatto, and P. Monk. Hexahedral $H(\text{div})$ and $H(\text{curl})$ finite elements. *ESAIM: M2AN*, 45:115–143, 2011.
- [10] M. Gyimeisi and D. Ostergaard. Non-conforming hexahedral edge elements for magnetic fields. *IEEE Trans. Mag.*, 34:2481–2484, 1998.
- [11] R. B. Lehoucq, D. C. Sorensen, and C. Yang. ARPACK users’ guide: Solution of large-scale eigenvalue problems by implicitly restarted Arnoldi methods, 1998.
<http://www.caam.rice.edu/software/ARPACK/>.
- [12] P. Monk. *Finite Element Equations for Maxwell’s Equations*. Oxford University Press, 2003.
- [13] J. Nédélec. Mixed finite elements in \mathbb{R}^3 . *Numer. Math.*, 35:315–341, 1980.
- [14] D. Sun, J. Mages, X. Yan, and Z. Cendes. Spurious modes in finite-element methods. *IEEE Antennas Propagat. Mag.*, 37:12–24, 1995.
- [15] S. Zaglmayr. ‘High order finite element methods for electromagnetic field computation’, PhD thesis, Johannes Kepler University of Linz, 2006.